PCCP

ROYAL SOCIETY OF CHEMISTRY

PAPER

View Article Online
View Journal | View Issue

Cite this: *Phys. Chem. Chem. Phys.*, 2021, **23**, 22352

Phenolic compounds alter the ion permeability of phospholipid bilayers *via* specific lipid interactions†

Sheikh I. Hossain, [a] Suvash C. Saha [b] and Evelyne Deplazes *[ac]

This study aims to understand the role of specific phenolic–lipid interactions in the membrane-altering properties of phenolic compounds. We combine tethered lipid bilayer (tBLM) electrical impedance spectroscopy (EIS) with all-atom molecular dynamics (MD) simulations to study the membrane interactions of six phenolic compounds: caffeic acid methyl ester, caffeic acid, 3,4 dihydroxybenzoic acid, chlorogenic acid, syringic acid and *p*-coumaric acid. tBLM/EIS experiments showed that caffeic acid methyl ester, caffeic acid and 3,4 dihydroxybenzoic acid significantly increase the permeability of phospholipid bilayers to Na^+ ions. In contrast, chlorogenic acid, syringic acid and *p*-coumaric acid showed no effect. Experiments with lipids lacking the phosphate group show a significant decrease in the membrane-altering effects indicating that specific phenolic–lipid interactions are critical in altering ion permeability. MD simulations confirm that compounds that alter ion permeability form stable interactions with the phosphate oxygen. In contrast, inactive phenolic compounds are superficially bound to the membrane surface and primarily interact with interfacial water. Our combined results show that compounds with similar structures can have very different effects on ion permeability in membranes. These effects are governed by specific interactions at the water–lipid interface and show no correlation with lipophilicity. Furthermore, none of the compounds alter the overall structure of the phospholipid bilayer as determined by area per lipid and order parameters. Based on data from this study and previous findings, we propose that phenolic compounds can alter membrane ion permeability by causing local changes in lipid packing that subsequently reduce the energy barrier for ion-induced pores.

Received 16th July 2021,
Accepted 27th September 2021

DOI: 10.1039/d1cp03250j

rsc.li/pccp

1. Introduction

Characterising how small molecules interact with biological membranes is critical for understanding fundamental processes and is relevant to many applications in pharmacology, biotechnology, and biomedical sciences. Examples include the membrane permeability of pharmaceuticals or endogenous substances such as hormones or neurotransmitters,[1–3] or the use of organic molecules in the cryopreservation of plant germplasm.[4,5]

Studying small molecule–membrane interactions (SMMIs) is challenging for several reasons. Cellular membranes are complex, supra-molecular structures composed of a phospholipid bilayer with embedded membrane proteins. The phospholipid bilayer contains hundreds of different lipids that are laterally diffusing, meaning that membranes provide a heterogeneous and constantly changing binding surface. Small molecules bound to membranes often do not show a single binding mode but several binding modes of similar energies, resulting in a frequent interchange between them. The amphipathic structure of phospholipids also creates two distinctly different environments for small molecules to interact with; the hydrophobic core and the more hydrophilic lipid–water interface. Furthermore, SMMIs can range from simple surface binding or passive diffusion across the membranes to more complex mechanisms such as membrane destabilisation or pore formation. Finally, the structure of a phospholipid bilayer can change in response to environmental conditions such as temperature, pH, ionic strengths, or hydration levels. As a result of this complexity, characterising SMMIs requires complementary information from different methods.

A wide range of wet-lab and *in silico* methods have been used to study the structure of membranes and their interactions with small molecules.[6–11] Molecular Dynamics (MD) simulations are routinely employed to provide atomistic-level insight into the structural, dynamical, and morphological properties of lipid

[a] *School of Life Sciences, University of Technology Sydney, Ultimo, NSW 2007, Australia. E-mail: e.deplazes@uq.edu.au*
[b] *School of Mechanical and Mechatronic Engineering, University of Technology Sydney, Ultimo, NSW 2007, Australia*
[c] *School of Chemistry and Molecular Biosciences, University of Queensland, St Lucia, QLD 4072, Australia*

† Electronic supplementary information (ESI) available. See DOI: 10.1039/d1cp03250j

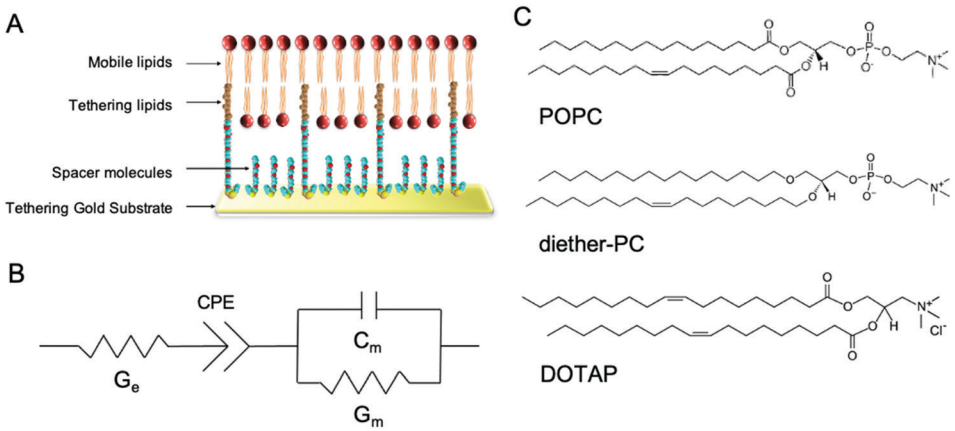

Fig. 1 Architecture of tethered bilayer lipid membranes (tBLM) and structure of the phospholipids used in the tBLM/EIS experiments. (A) tBLMs are formed on a gold substrate covered by spacer and tethering molecules, on which a phospholipid bilayer is formed. (B) The equivalent circuit is used to model tBLMs where G_e is the conduction of the electrolyte solution, G_m is the membrane conduction, and C_m is the membrane capacitance. CPE is the constant phase element representing the buffer reservoir and gold tethering electrode. (C) tBLMs were composed of POPC, diether-PC or DOTAP lipids.

membrane systems, including the effect of small molecules on these properties.[10,12–14] MD simulations are particularly useful when the properties of interest are inaccessible or difficult to access by wet-lab techniques. A compelling approach is to combine MD simulations with wet-lab techniques that provide complementary information. Ideally, the systems used in the simulations and wet-lab experiments should match with respect to phospholipid bilayer composition, pH and concentration and type of ions present.

In this study, we demonstrate the use of tethered lipid bilayer (tBLM) electrical impedance spectroscopy (EIS) combined with MD simulations to study SMMIs. tBLM/EIS is a technique to monitor the ion permeability of phospholipid bilayers in real-time. A tBLM is formed by anchoring tether molecules to the surface of a pure gold substrate (Fig. 1A). The tethers are interspersed with spacer molecules. Onto this sparsely tethered monolayer, a mobile phospholipid bilayer is formed using a solvent exchange technique. The resulting bilayer consists of 90% freely mobile phospholipids in the inner leaflet and 100% mobile phospholipids in the outer leaflet and thus mimics the fluidity of cell membranes. If a potential gradient is applied, the bilayer acts as an impediment to the movement of ions in the buffer, which can be measured using swept frequency EIS. The resulting impedance and phase data are fitted to an equivalent circuit (Fig. 1B) to obtain a measure of membrane conductivity.[15] An increase in conduction upon treating a membrane with a specific compound reflects an increase in ions moving across the membrane, *i.e.*, an increase in the permeability of the lipid bilayer towards ions. The underlying assumption of our EIS experiments that increased ion permeability is the result of changes in lipid packing or other local changes in membrane structures, which make it easier for ions to move through the bilayer.[16–18]

In this study, tBLMs were composed of the neutral phospholipids POPC and dietherPC or the positively charged lipid DOTAP. Diether-PC and DOTAP are structurally similar to POPC but lack the ester (carbonyl) oxygens or the phosphate group, respectively (Fig. 1C). Comparing the conduction between membranes composed of POPC, diether-PC and DOTAP treated with the same compounds allows insight into how specific interactions at the water–lipid interface affect membrane disruption.

We instigated the membrane interactions of the following six phenolic compounds: caffeic acid methyl ester (CAME, also called methyl caffeate), caffeic acid (CA), 3,4 dihydroxybenzoic acid (DHBA), chlorogenic acid (CGA), syringic acid (SGA) and *p*-coumaric acid (*p*CA). The structures of these six compounds are shown in Fig. 2. We selected these six compounds based on our work studying the membrane-altering effects of honey.[19] All these phenolic compounds are found in honey.[20–23] Further,

Evelyne Deplazes

Dr Evelyne Deplazes is a Senior Lecturer at the University of Queensland and an Adjunct Research Fellow at the University of Technology Sydney. She received her PhD in computational biophysics from the University of Western Australia in 2012. She then carried out postdoctoral work at the University of Queensland and Curtin University, funded by early-career fellowships from the Swiss National Science Foundation and the Australian National Health and Research Council. In 2019, she started her independent research group at the University of Technology Sydney, which she now continues at the University of Queensland after taking up a position as Senior Lecturer in 2021. Her lab combines molecular simulations and biophysical chemistry experiments to study how small molecules and peptides interact with biological membranes and membrane proteins. The knowledge and tools from her research help develop new pharmaceuticals and understand fundamental processes such as membrane permeation or pore formation.

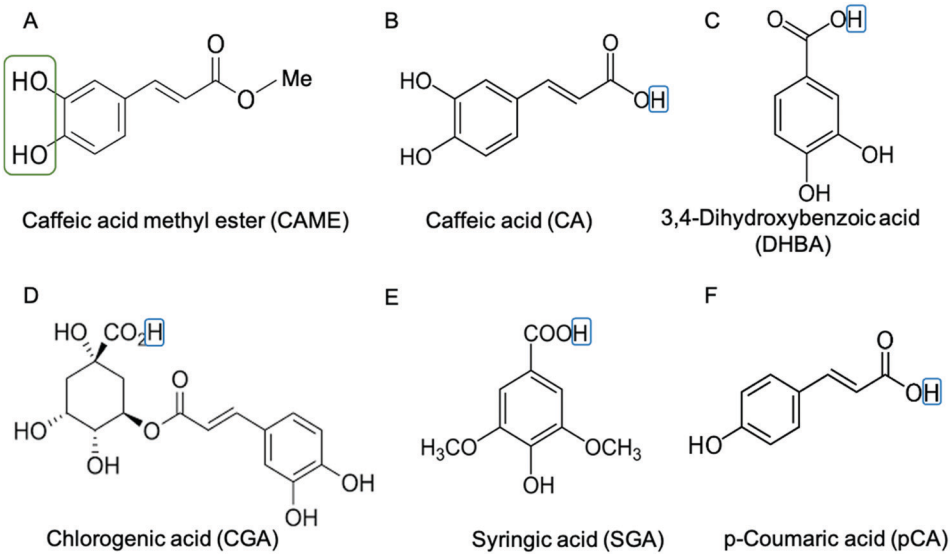

Fig. 2 Structure of phenolic compounds used in this study. (A) Caffeic acid methyl ester (CAME), (B) caffeic acid (CA), (C) 3,4-dihydroxybenzoic acid (DHBA), (D) chlorogenic acid (CGA), (E) syringic acid (SGA) and (F) *p*-coumaric (*p*CA). The catechol group is indicated by a green box in (A) CAME. The catechol group is also present in CA, DHBA and CGA. The hydrogen of the carboxylic acid is indicated by a blue box. For CA, DHBA, CGA, SGA and *p*CA this hydrogen was removed for simulation, *i.e.*, the compounds are simulated in their deprotonated (anionic) form, giving them a charge of −1.

the six compounds are similar in structure and physicochemical properties. Thus, understanding differences in their membrane-altering properties requires detailed structural information and makes these compounds an ideal set to study by combined tBLM/EIS and MD simulations.

Phenolic compounds are a diverse class of aromatic molecules found in plants that have been extensively investigated for their biological activity and potential applications in the pharmaceutical, cosmetics and food industries. For example, CA and CGA show antioxidant, anticancer and anti-inflammatory activities.[24–27] CA also offers protective effects against oxidising agents in red blood cells by preventing morphological changes and lysis.[28] Phenolic compounds also have metal-chelating properties where the complexation occurs by the metal interacting with the hydroxyl or catechol group.[29–31] In many cases, the antioxidant activities of the phenolic compounds and metal chelation are related.[32] For example, the catechol motif escalates the antioxidant activity compared to a single hydroxyl group.[32]

Some of the biological activities of phenolic compounds relate to their interactions with the phospholipid bilayer component of membranes.[33–35] These membrane-related activities are associated with specific lipid–phenolic interactions (*e.g.* in preventing lipid peroxidation[36]) and with non-specific effects by altering the biophysical properties of the membrane.[33,37] For example, a recent *in vitro* study reported that the hydration state of the lipid interface affects the antiradical activity of CAG.[38] The biological activity of phenolic compounds is also affected by lipid composition[33,35,39] and the location of the compound in the membrane.[33,39] These studies highlight the complexity of phenolic–membrane interactions and demonstrate how characterising them can assist in understanding their biological activity and inform their use in various applications.

2. Methods and materials

2.1. tBLM/EIS experiments

Materials. 1-Palmitoyl-2-oleoyl-*sn-glycero*-3-phosphocholine (POPC), 1,2-di-*O*-(9*Z*-octadecenyl)-*sn-glycero*-3-phosphocholine (diether-DOPC) and 1,2-dioleoyl-3-trimethylammonium-propane (DOTAP) were purchased from Avanti Polar Lipids Inc., through their Australian distributor Sigma-Aldrich Corporation. Sodium chloride, ethanol, tris(hydroxymethyl)-aminomethane (Tris), caffeic acid, chlorogenic acid, 3,4 dihydroxybenzoic acid, syringic acid and *p*-coumaric acid were obtained from Sigma-Aldrich Corporation. Caffeic acid methyl ester (methyl caffeate) was obtained from Saphira Biosciences Australia. All phenolic compounds were obtained as solids and had a purity of 95% or higher. The electrodes and equipment to form the tethered phospholipid bilayers were purchased from SDx Tethered Membranes, Pty Ltd, Sydney, Australia. TethaPod™ and tethaQuick™ for EIS were supplied by SDx Tethered Membranes, Pty Ltd, Sydney, Australia.

Buffers and phenolic compound solutions. tBLMs were formed using a tris buffer composed of 10 mM Tris 100 mM NaCl. The pH of the buffer was adjusted to 7.0 ± 0.1 by dropwise addition of 1 M HCl. All phenolic compounds were dissolved at 500 ppm in tris buffer, and the pH was adjusted to 7.0 ± 0.1 by dropwise addition of 1 M NaOH.

Tethered bilayer lipid membrane arrays (tBLMs). Tethered lipid bilayer membranes were formed following a standard solvent-exchange procedure.[15] Briefly, tBLMs were made using gold slides coated with a T10 architecture, which consists of 10% tethers made of benzyl-disulphide-eleven-oxygen-ethylene-glycol reservoir linkers with a C20 phytanyl group, and 90% spacers made of four-oxygen-ethylene-glycol reservoir linkers with a terminal OH group (catalogue reference T10™, SDx

Tethered Membranes Pty Ltd, Sydney, Australia). The phospholipid bilayer was formed using a solvent-exchange technique[15] with 3 mM ethanolic solutions of either POPC, diether-PC or DOTAP lipids. Lipids were left to incubate with the tethering monolayer for 2 min before a rapid exchange of 2 × 400 μL tris buffer to induce the formation of the mobile phospholipid bilayer. A detailed protocol for the formation of tBLMs can be found in Cranfield *et al.*[15]

Electrical impedance spectroscopy. The conductance (G_m) of the tBLMs were measured with a tethaPod™ swept-frequency impedance spectrometer employing real-time modelling of the impedance profiles using the tethaQuick™ software. A resistor–capacitor model was chosen to describe G_m (see the equivalent circuit in Fig. 1C). A sequence of 25 mV peak to peak excitation periods was applied within the frequencies 0.1 Hz to 2 kHz using four steps per decade. With these settings, a sweep is between 70 to 80 seconds. For a detailed description of AC impedance spectroscopy methods used, refer to Cranfield *et al.*[15]

After formation, the tBLM was washed at least three times with 200 μL tris buffer or until a stable baseline conductance was achieved where stable was considered at least five readings with no more than 10% variation in absolute conductance.

To measure the effect of phenolic compounds on conductance, an experiment consisted of the following addition-washout protocol. A single addition – washout cycle consisted of one addition, followed by two buffer washouts. For the addition, 200 μL of the 500 ppm phenolic compound solution was added to the wells, and the tBLM was left for at least 10 sweeps. For the washout, the 200 μL of tris buffer was added to wells, and the tBLM was left for at least 10 sweeps, followed by an identical second washout. This addition – washout cycle was repeated. For each phenolic compound, at least four independent experiments on separate membranes were conducted.

Data analysis. Changes in membrane conductance upon the addition of phenolic solution are reported as normalised conductance. For this, the membrane conductance of each tBLM was normalised using a dedicated baseline value, which was calculated by averaging the conductance of the last 10 sweeps before the first addition of the phenolic solution. The conductance reading used for comparative analysis was the normalised conductance after the second addition, averaged over 5 sweeps. Normalised conductance values are reported as averages ± standard error of the mean.

Unpaired *t*-tests were used to determine the difference in membrane conduction between experiments of a given phenolic compound on tBLMs composed of different lipids. All statistical analyses were carried out using Orange version 3.29.1.

2.2. MD simulations

Parameters for phenolic compounds. All simulations were carried out to mimic neutral pH. The pK_a for CA, DBHA, SGA, CGA, and *p*CA is <5.0, meaning that at neutral pH, the carboxylic acid will predominantly be present in the deprotonated state (the implications of this are described in the discussion). These acids were thus parameterised in their anionic form with a charge of −1.0. CAME lacks the carboxylic acid is thus parameterised in its neutral form. Parameters for all compounds were derived from Antechamber in AMBER Tools v. 20.[40] Atom types from the general amber force field (GAFF)[41] with restrained electrostatic potential (RESP)[42] charges were used. Each compound was geometry optimised, and the electrostatic potential was calculated with Gaussian 09[43] at HF/6-31+G* level of theory and the polarisable continuum model (PCM) with default settings. The RESP charges were fitted using Antechamber. Topology and structures were converted to GROMACS file formats with the acpype.py script.[44] For CGA, the calculated octanol–water free energy of transfer using these parameters was significantly overestimated, resulting in deviations from the reported partition coefficient. The partial charges were adapted to increase the polarity of the compound and thus decrease the partition coefficient.

Calculation of octanol–water partition coefficients for phenolic compounds. For each of the six compounds, the octanol–water partition coefficient $P_{w\to o}$ was calculated using the following relationship:

$$\log P_{w\to o} = \frac{\Delta G_{w\to o}}{2.303RT}$$

where $\Delta G_{w\to o}$ is the Gibbs free energy of moving the compound from the water to the octanol phase, $R = 8.314$ J mol^{-1} K^{-1} is the universal gas constant, and T is the temperature in Kelvin (298 K).

$\Delta G_{w\to o}$ was obtained from the potential of mean force (PMF), which was calculated using umbrella sampling (US). The distance between the centre of mass (COM) of the phenolic compound and the COM of the octanol phase along the *z*-axis of the simulation system was used as a reaction coordinate. The simulation system consisted of a pre-equilibrated water–octanol system that contained 5417 water molecules and 310 octanol molecules in a rectangular box of dimension 5 nm × 5 nm × 10 nm. To this, one phenolic compound was added. To create a series of starting structures for the US simulations, a 2 ns pull simulation in the *NPT* ensemble was carried in which the phenolic compound was moved along the reaction coordinate with a force constant of 1000 kJ mol^{-1} nm^{-2} and a pull rate of 2 nm ns^{-1}. From the resulting trajectory, 20 configurations with phenolic–octanol COM distances between 0 and 4.0 nm were extracted. For the US simulations, 20 windows were simulated for 100 ns, each using the same *NPT* settings as for the pull simulation. Windows were separated by 0.2 nm, and the position of the phenolic compound was restrained along the reaction coordinate with a force constant of 1000 kJ mol^{-1} nm^{-2}. The PMF was reconstructed using the weighted histogram analysis method (WHAM),[45] and the statistical error was estimated using bootstrapping analysis method.[46,47] The $\log P_{w\to o}$ values obtained from the US simulations are listed in Table S1 in the ESI,† along with experimental values.

Simulations of POPC with phenolic compounds. First, a POPC-only system was built using a POPC bilayer containing

512 lipids. The system also contained 42 377 water molecules, 77 Na^+ and 77 Cl^- ions in a rectangular box with dimensions ~13 nm × 13 nm × 11.5 nm. This corresponds to an ionic strength of 100 mM NaCl. The system was energy minimised using the steepest descent algorithm and equilibrated for 500 ns in an *NPT* ensemble. Equilibration was monitored using area per lipid (APL) *vs.* time. This POPC-only system later served as a reference system for analysis.

The last frame from the POPC-only simulation was used as the starting structure for all POPC-phenolic simulations. In total there were six simulation systems: one for each phenolic compound. For each system, 10 phenolic compounds were added by replacing randomly selected water molecules. In the case of CA, SYG, DHBA, *p*-CA and CGA, 10 additional Na^+ ions were added to neutralise the system. Each system was again energy minimised, followed by a 500 ns *NPT* run.

All systems were simulated using GROMACS versions 2020.3[48] and GROMACS 2020.4.[49] POPC, water and ions were described using Lipid14, TIP3P water[50] and ions and the Amber force field.[51] Periodic boundary conditions were applied in all directions of the simulation system. Non-bonded interactions were modelled by Lennard-Jones and Coulomb potentials with a cut-off of 1.0 nm and 0.12 nm grid spacing. The neighbour list was updated every 20 steps. Electrostatic interactions were calculated using the PME method.[52] The equation of motion in all the simulations was integrated using the Verlet algorithm[53] with 2 fs time step size. The system components POPC, water with ions and phenolic compounds were coupled independently to a Nose–Hoover thermostat[54] with a bath temperature of 298 K and a time constant of 0.1 ps. The POPC and solute were coupled separately to the water and ions. A Parrinello–Rahman barostat[55] with semi-isotropic pressure coupling was applied using a time constant of 2 ps and compressibility of 4.5×10^{-5} bar^{-1} in all directions of the simulation box.

Simulations were analysed using GROMACS tools, Visual Molecular Dynamics (VMD)[56] and python scripts using the MDAnalysis package.[57] Unless otherwise stated, all analyses were carried out using frames from the last 200 ns of the 500 ns simulation. The minimum distance between any atom in a phenolic compound and the POPC phosphate oxygen was calculated using *gmx mindist*. The orientation between the phenolic compound and the membrane surface was estimated by the angle formed between the bilayer normal that runs along the *z*-axis of the simulation system and a vector connecting two atoms in the phenolic compound. The atoms used to define these vectors are shown in Fig. S1 in the ESI.† As the compounds have free rotation in solution, the distributions of orientation angles were calculated using only compounds that are within 0.8 nm of the membrane surface (as defined by the phosphate oxygen in POPC). The insertion depth of each phenolic compound is defined by the distance between the *z*-component of the membrane COM and two atoms at opposing ends of the phenolic compound (referred to as the head and tail of the compound[58]). The atoms that define head and tail are shown in Fig. S2 in the ESI.†

3. Results

3.1. tBLM/EIS data

Fig. 3 shows representative traces of normalised conductance *vs.* time for tBLMs composed of POPC that were treated with 500 ppm solutions of CAME, CA, DBHA, CGA, SGA and *p*CA, respectively. The treatment consisted of adding the phenolic compound solution (add), followed by two washes with tris buffer (wash). For all experiments, the conductance of a control membrane treated with buffer only was recorded (indicated in Fig. 3B). Note that an increase in conductance reflects an increase in ions moving through the membrane. Conductance is thus not a measure of the permeability of the phenolic compound but of the permeability of the membrane towards ions.

Comparison between the conductance traces shows substantial variations in how the six phenolic compounds affect the ion permeability of a POPC bilayer. CAME, CA and DBHA show an increase in conductance while CGA, SGA and *p*CA show no such effect. Further, a comparison of the conductance traces from CAME, CA and DBHA suggests that there are differences in the mechanism of how these compounds alter membrane ion permeability. Addition of CAME causes a significant and rapid increase in normalised conductance from a baseline of 1.0 ± 0.0 to 19.1 ± 0.3 ($p < 0.001$). After the first washout, conductance drops to 5.0 ± 0.2, and after the second washout, further drops to 2.4 ± 0.1. The same pattern is observed in the second treatment cycle. These results suggest that CAME significantly affects membrane permeation but the effect is reversible once the compound is washed out.

For CA, the first addition causes a sudden increase in normalised conductance to 3.0 ± 0.1. Each washout causes a further, small increase of conductance, which continues for the second treatment cycle. The final, normalised conductance after the two treatment cycles is 10.2 ± 0.3. This is significantly higher than baseline conductance ($p < 0.001$) but lower than the levels reached with CAME ($p < 0.01$). Thus, compared to CAME, CA has less effect on membrane ion permeation but changes to the membrane appear more permanent.

For DHBA the onset of the increase in conduction is even slower than for CAME and CA. After the first treatment cycle, the normalised conductance is 1.1 ± 0.1, which is the same as the normalised conductance for control experiments 0.97 ± 0.04. The conductance continues to increase with each addition of DHBA or buffer washout, reaching a final conductance of 2.7 ± 0.3. As for CA, the conductance data for DHBA suggests that the compound remains in the membrane even after buffer washout.

For the three phenolic compounds that caused membrane disruption, the tBLM/EIS experiments were repeated using bilayers composed of diether-PC or DOTAP. These two lipids lack the ester (carbonyl) oxygens or the phosphate group, respectively (Fig. 1C). Fig. 4 reports the normalised conductance reached after the second addition of the phenolic compound to bilayers composed of POPC, diether-PC or DOTAP. For CAME, replacing the POPC with dietherPC or DOTAP significantly

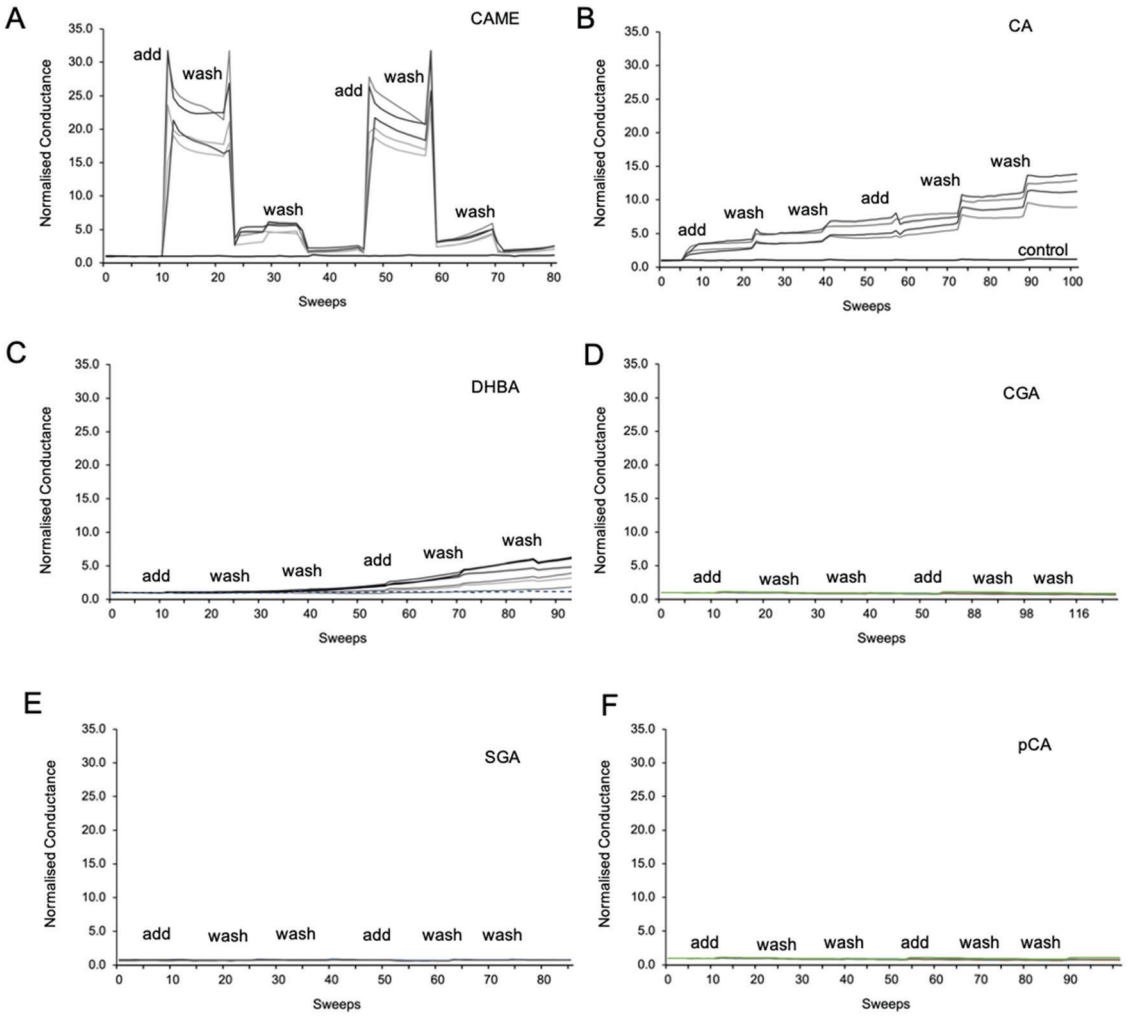

Fig. 3 Representative traces of normalised conductance *vs.* time for tBLMs treated with caffeic acid methyl ester (CAME, A), caffeic acid (CA, B), 3,4 dihydroxybenzoic acid (DBHA, C), chlorogenic acid (CGA, D), syringic acid (SGA, E) and *p*-coumaric acid (*p*CA, F). The treatment protocol consisted of adding phenolic compound solution (add), followed by two washes with tris buffer (wash). 1 sweep is equal to 70–80 seconds. All tBLMs were composed of POPC lipids. The concentration of all phenolic acids was 500 ppm, and solutions were adjusted to pH 7. For all experiments, the conductance of a control membrane treated with buffer only was recorded (indicated in B).

reduces conductance from 19.1 ± 0.3 to 15.6 ± 0.2 and 2.7 ± 0.2, respectively. For CA, the conductance does not significantly differ between POPC and dietherPC (7.8 ± 0.2 compared to 9.9 ± 0.8). In contrast, the conductance for DOTAP is significantly reduced to 0.3 ± 0.8, which is even below baseline conductance. Finally, for DHBA, the conductance is significantly reduced for both dietherPC and DOTAP from 2.7 ± 0.8 and 1.1 ± 0.0, respectively.

3.2. Simulations

Effect of phenolic compounds on membrane structure. The area per lipid (APL) and lipid order parameters were used to assess whether the binding of the phenolic compounds affects the overall structure of the phospholipid bilayer. The results show that there is no significant change in APL or order parameters in the POPC bilayer for any of the compounds (see Table S2 and Fig. S3 in the ESI†).

Proximity of phenolic compounds to the membrane surface. Table 1 shows the % of frames each of the compounds is close to the membrane surface. A phenolic compound was considered close to the membrane surface if any of the atoms in the compound were within 0.2 nm of the POPC phosphate atoms. The data was calculated separately for each of the ten compounds in the system and then averaged using data from the last 200 ns of the 500 ns simulation. It is evident that CAME, CA and DHBA spend significantly more time near the membrane surface than SGA and *p*CA (95% confidence interval). CAME molecules are found close to the membrane surface for 99% of the simulation time. Similarly, CA and DHBA are located close to the membrane surface >90% of the time. For *p*CA and SGA, the time spent bound to the membrane is only 39% and 12%, respectively. The results for CGA show a much higher standard deviation than the other compounds and prompted us to take a closer look at the data from the 10 individual CGA molecules in the system (Table S3 in the ESI†). Seven of the 10 molecules are

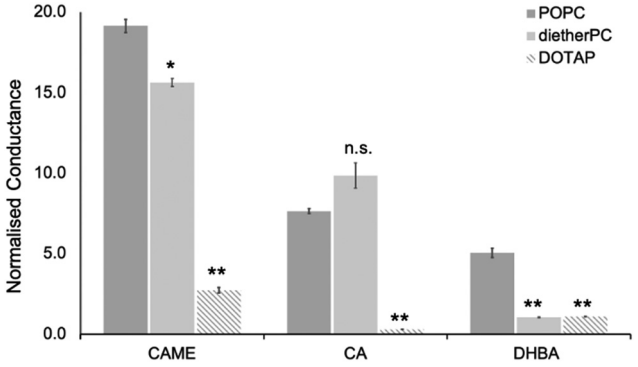

Fig. 4 Effect of caffeic acid methyl ester (CAME), caffeic acid (CA) and 3,4 dihydroxybenzoic acid (DBHA) on tBLMLs composed of POPC, diether-PC or DOTAP. The concentration of all phenolic acids was 500 ppm, and solutions were adjusted to pH 7. The normalised conductance reported is the average reached after the second addition of phenolic solutions, which are averaged over at least 4 independent experiments. Error bars are ±standard error of the mean. * = $p < 0.05$, ** = $p < 0.01$. n.s. = not statistically significant.

bound to the membrane surface 100% of the time, while the other three molecules are bound 0, 3 or 44% of the time. Visual inspection of the trajectory showed that these three molecules interact with other CGA molecules bound to the surface but remain in the water phase (Fig. S4 in the ESI†). Thus, while these molecules are close to the membrane surface, they do not form direct interactions with the lipids or interfacial water.

An interesting point can be made when considering the time spent in proximity of the membrane alongside the partition coefficients (log *P*). The log*P* values predicted from the free energy calculations for DHBA, CA, SGA and *p*CA are, in increasing order, 0.5, 0.98, 1.05 and 1.1. This order does not agree with their order of time spent close to the membrane surface: SGA ≪ *p*CA ≪ DHBA ≈ CA. The discrepancies between log*P* and membrane proximity are particularly strong when comparing CA, SG and *p*CA. Their log*P* values are very close, yet their time spent close to the membrane range from >90% for CA to 12% for SGA. These large differences are a first indication that log*P* values are not a reliable indicator to predict surface interactions for these phenolic compounds, which will be outlined in more detail in the discussion.

Table 1 Proximity to membrane surface. A phenolic compound was considered bound to the membrane surface if any of its atoms were within 0.2 nm of the POPC phosphate atom. Percentages were calculated separately for each compound using the last 200 ns of the 500 ns simulation and averaged over the 10 compounds in the system. Errors are given as standard deviations

Phenolic compound	Percentage of frames
CAME	99.48 ± 1.37
CA	91.39 ± 11.28
DHBA	92.10 ± 4.95
CGA	74.81 ± 40
SGA	12.72 ± 3.44
*p*CA	39.69 ± 6.94

Insertion depth. To investigate the location of the phenolic compounds with respect to the membrane surface, we calculated the insertion depth of each phenolic compound (Fig. 5). Insertion depth was estimated by the distance between two selected atoms in the phenolic compound and the COM of the membrane in the *z*-dimension, $\langle \Delta z \rangle$. Rather than using the COM of the phenolic compound, $\langle \Delta z \rangle$ was calculated for two selected atoms at opposing ends of the molecule to the COM of the membrane.[58] These atoms in the phenolic compound designate the head and tail (Fig. S2 in the ESI†). Distances were averaged over the last 200 ns of the 500-ns simulation and over the 10 phenolic compounds. Fig. 5 shows $\langle \Delta z \rangle$ for all six phenolic compounds. As a reference, the figure also depicts the average *z*-position of the nitrogen, phosphate, or carbonyl oxygen atoms in POPC. Comparison of $\langle \Delta z \rangle$ for the six compounds shows that CAME is the most embedded in the membrane, sitting at the level of the carbonyl oxygen at the top of the hydrophobic core of the membrane. CA and DHBA are localised close to the headgroups at the water–lipid interface. The remaining three phenolic compounds, CGA, SGA and *p*CA, are positioned above the headgroups, further away from the water–lipid interface. None of the compounds penetrate the hydrophobic core of the membrane.

Orientation of phenolic compounds. The orientation of the phenolic compound with respect to the membrane surface was determined by the angle formed between the *z*-axis of the simulation system, which is normal to the bilayer, and a vector connecting two atoms at opposing ends of the phenolic compounds (see also Fig. S1 in the ESI†). Fig. 6 shows the normalised probability distributions of the orientation angle α. The distributions represent the combined data from the 10 compounds in the respective simulation systems. As the compounds have free rotation in solution, the distributions of orientation angles were only calculated for compounds that are close to the membrane surface. A value of $\alpha = 0^\circ$ or 180° indicates that the vector running along the phenolic compound runs parallel to the bilayer normal (*i.e.*, the compound is at the right angle with respect to the membrane surface). A value of $\alpha = 90^\circ$ means the vector running along the phenolic compound is parallel to the membrane surface.

Comparison of the distributions shows that CAME and CGA have a unimodal distribution with a slight preference for orientations close between $\sim 60^\circ$ to $\sim 120^\circ$ with the most preferred orientation at $\alpha = 90^\circ$. In contrast, CA, *p*CA and DHBA show bimodal distributions with a maximum of around $\alpha = 40^\circ$ and $\alpha = 140^\circ$ to 150°. SGA shows the broadest distribution. Note that the spikes in CAME, CA and SGA are caused by two or three compounds that stay in specific orientations for long periods of time, biasing the distributions. Overall, the analysis shows that except for SGA, all phenolic compounds show a preferred orientation with respect to the membrane surface.

Cluster formation. We carried out cluster analysis to compare the aggregation properties of the phenolic compounds. Two or more phenolic compounds were considered as part of a cluster if their COM are within 1.5 nm of each other. Table 2 lists the % of frames during which two, three or four molecules are found in a

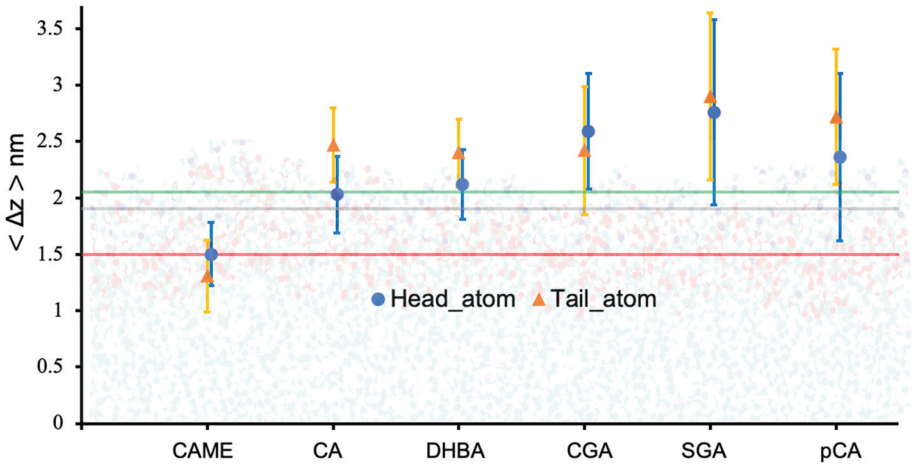

Fig. 5 Insertion depth for phenolic compounds, estimated by the average distance $\langle \Delta z \rangle$ of the head and tail of phenolic compounds to the COM of the POPC bilayer. The atoms defining the head and tail of each phenolic are shown in Fig. S2 of the ESI.† The three horizontal lines represent the average position of the nitrogen (green), phosphate (grey) and carbonyl (orange) atoms in POPC. All values were calculated from the last 200 ns of the 500 ns production run and averaged over the 10 compounds. Error bars represent standard deviations.

cluster. CAME has the strongest tendency to aggregate, and for 32% of the simulation time, two compounds are in proximity of each other. Visual inspection shows that the aggregation occurs in a way such that both CAME molecules in the cluster are bound to the membrane surface, consistent with the fact that CAME spends 99% of the simulation time proximal to the membrane surface. Clusters with three CAME molecules are much less likely and only occur 4% of the time. Compared to CAME, all other compounds show a much smaller or no tendency to aggregate. CA, SGA and *p*CA are found in clusters with two molecules only 6%, 4% and 3% of the simulation time, respectively. DHBA shows no clustering at all. In contrast, CGA shows a very strong tendency to form clusters of four molecules. As noted in the previous section, CGA aggregates in a way such that one or two molecules are superficially bound to the membrane surface while the other molecules in the cluster remain in the water phase (Fig. S4 in the ESI†). Visual inspection shows that these clusters are long-lived and stable over >400 ns of the 500 ns simulation.

Phenolic–lipid and phenolic–water coordination at the lipid–water interface. Fig. 7 shows the most common interactions formed by CAME, CA and DHBA, which we refer to as binding modes. To identify the dominant binding modes, the interactions of all 10 compounds in the system with lipids and water molecules were analysed. For phenolic compound–lipid interactions, we distinguished between the phosphate oxygen and carbonyl oxygen.

The most common binding mode for CAME involves the catechol group interacting with the phosphate oxygen and the methyl ester surrounded by interfacial water. This mode accounts for 84% of binding events. A similar binding mode is observed for CA and DHBA. Like CAME, both compounds show a preference for the phosphate group, and the most common binding mode is the catechol interacting with the phosphate oxygen and the carboxylic acid interacting with water. This mode accounts for 66% and 70% of binding events in CA and DHBA, respectively. In addition, both CA and DHBA show a binding mode where the catechol group is bound to the phosphate oxygen, and the carboxylic acid moiety interacts with both water and hydrogens in the lipid headgroup. These account for approximately 15% of interactions. Note, this binding mode of bridging two lipids is not possible for CAME. For all three phenolic compounds, less than 1% of interactions involve the lipid carbonyl oxygen.

The other phenolic compounds do not show such strong preferences for a specific binding mode. Also, *p*CA, SGA and CGA show much less interaction with lipid oxygens and prefer interfacial water instead. The most common binding mode for *p*CA is similar to CA and DHBA, where the hydroxyl group interacts with the phosphate oxygen, and the carboxylic acid interacts with water. This mode, however, only accounts for 30% of binding events. All other times when *p*CA is close to the membrane surface, the compound interacts with interfacial water. SGA shows even lower levels of interactions with lipids. Only 15% of interactions involve phosphate oxygen, and there are no interactions with carbonyl oxygen or other parts of the lipid. For SGA, the carboxylic moiety interacts exclusively with interfacial water, and there is very little interaction with the lipid oxygens. The catechol group in CGA shows no interaction with lipid oxygens and exclusively interact with interfacial water. While the hydroxyl and carboxylic acid groups in the non-aromatic ring show some interactions with the lipid phosphate oxygen, most interactions are with interfacial water.

4. Discussion

In this study we aimed to investigate the interaction of six phenolic compounds with phospholipid bilayers with a particular focus on the role of specific phenolic–lipid interactions in the compounds' ability to alter membrane ion permeability. For this, we used tBLM/EIS to compare the effect of six different phenolic

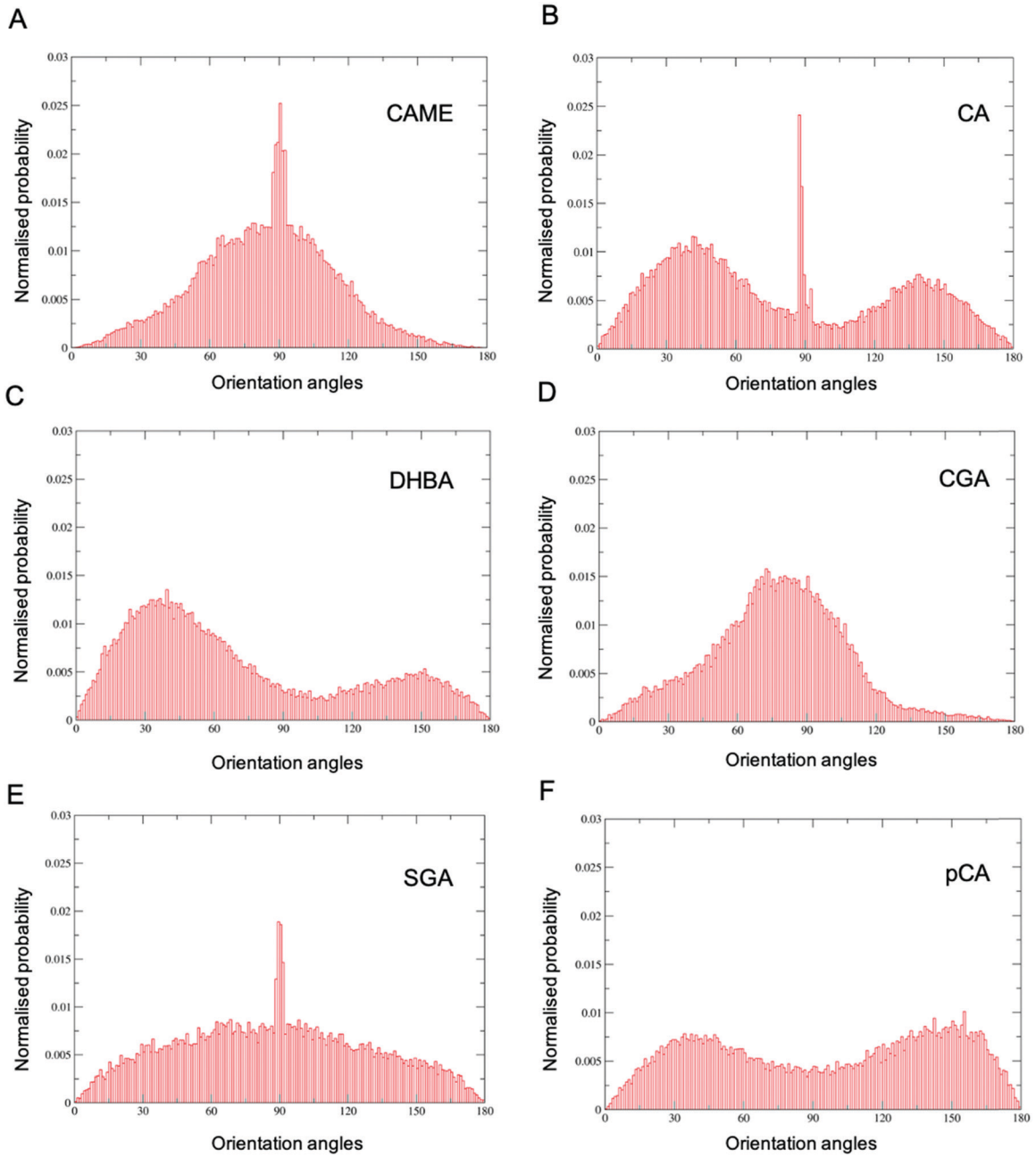

Fig. 6 Orientation of phenolic compounds (A) caffeic acid methyl ester (CAME), (B) caffeic acid (CA), (C) 3,4-dihydroxybenzoic acid (DHBA), (D) chlorogenic acid (CGA), (E) syringic acid (SGA) and (F) *p*-coumaric (*p*CA) when close to the POPC membrane surface. Distributions were calculated using the combined data from all 10 phenolic compounds in the system and all frames from the last 200 ns of the 500 ns simulation. The orientation is defined by a vector connecting two atoms in the compound and the *z*-axis of the simulation system.

compounds on the ion permeability of phospholipid bilayers composed of POPC. In addition, we used MD simulations of phenolic compounds in the presence of a POPC bilayer to provide information on the insertion depth, orientation, aggregation properties and phenolic–lipid interactions on each of the phenolic compounds.

The tBLM/EIS experiments revealed that of the six compounds, CGA, SGA and *p*CA do no alter the conductance in phospholipid bilayers membrane while CAME, CA and DHBA significantly increase conductance. Further, the time-dependent conductance traces from CAME, CA and DHBA suggest major differences in the mechanism by which these three compounds alter membrane ion permeability. Potential reasons for these differences will be discussed later in the context of results from the MD simulations.

In the EIS experiments, a weak electric field of 25 mV (0.025 V) peak to peak and 0 mV bias is applied. If the electric field would cause large disruptions when adding charged compounds to the membrane, we would see this for SYG, CGA and *p*CA as well. Our EIS data indicates that the disruption only occurs with selected compounds.

Table 2 Clustering of phenolic compounds on a POPC membrane surface. Two or more phenolic compounds were considered as part of a cluster if their COM are within 1.5 nm of each other. The % of phenolic compounds found in a cluster of two, three or four molecules were calculated from the last 200 ns of a 500 ns simulation

Phenolic compound	% frames during which two, three or four molecules are found in a cluster		
	2 molecules	3 molecules	4 molecules
CAME	32%	4%	0%
CA	6%	0%	0%
DHBA	0%	0%	0%
CGA	0%	1%	98%
SGA	4%	0%	0%
*p*CA	3%	0%	0%

As noted in the introduction, the underlying assumption of our tBLM/EIS experiments is that an increase in conductance reflects a change in ion permeability of the membrane, which is caused by the phenolic compound altering the packing of lipids in the bilayer. Under this assumption, an increase of conductance thus indicates a membrane disrupting effect. There are, however, other mechanisms that can cause an increase in conduction. For example, protonophores able to transport protons across membranes have been shown to increase conductance in phospholipid bilayers as measured by EIS.[59] Protonophores operate *via* a mechanism that does not necessarily require disruption of lipid packing. The anionic form of the protonophore adsorbs to the membrane surface, where it associates with protons to form a neutral form of the compound. There is ample evidence that protons accumulate on and move along water–lipid interface.[60–68] The protonated form is less polar and able to translocate across the hydrophobic core of the membrane. The compound dissociates again into the anionic protonophore, and protons are released on the other side of the membrane. In a tBLM/EIS experiment, this transport of protons across the membrane would cause an increase in conductance. While we cannot exclude that protonophore activity contributes to the increase in conductance, for the reasons outlined below, we think that the effect from the phenolic compounds is at least partially caused by disrupting the lipid packing and subsequent formation of water-filled pores rather than protonophore activity alone.

First, the only difference between CAME and CA is that in the former the carboxylic acid is replaced by a methyl ester (Fig. 2).

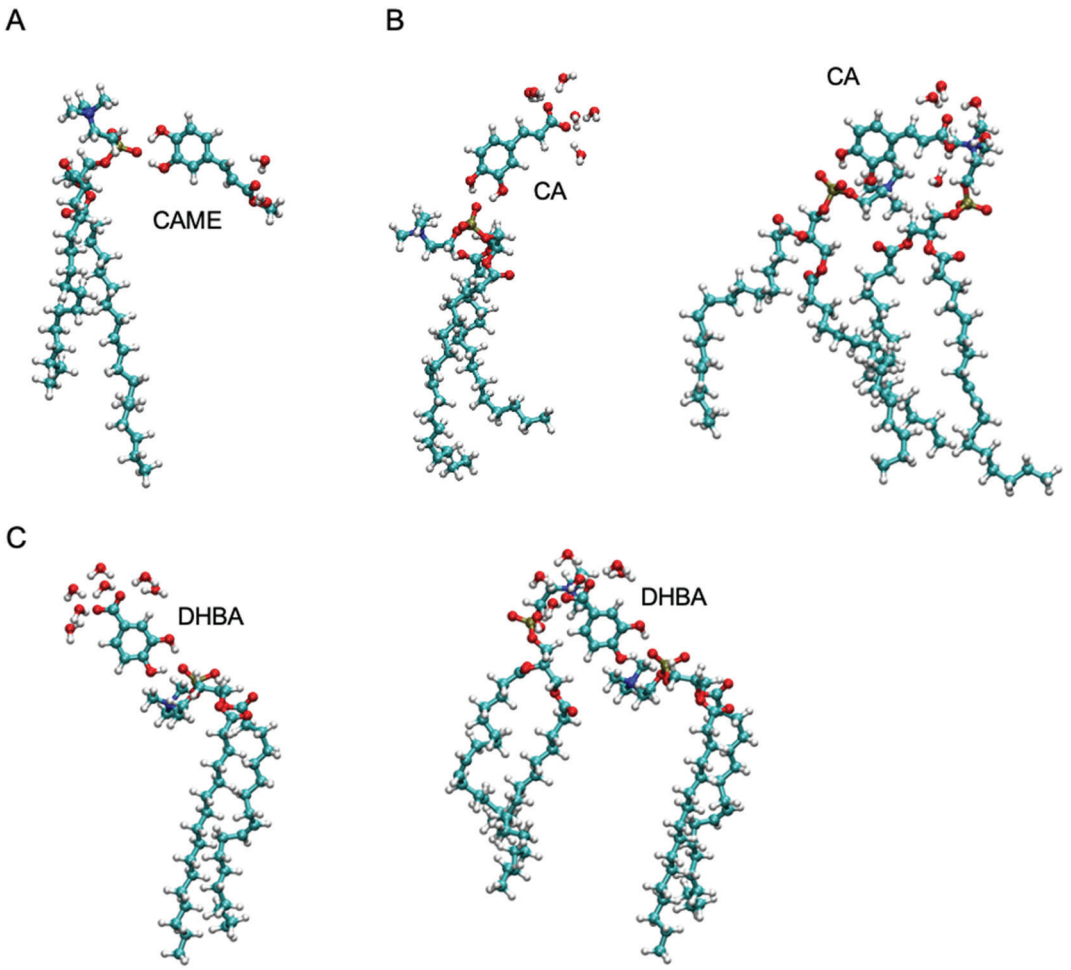

Fig. 7 The most common interactions formed by (A) caffeic acid methyl ester (CAME), (B) caffeic acid (CA) and (C) 3,4-dihydroxy benzoic acid (DHBA) with lipids and interfacial water.

If the increase in conduction by CAME and CA were caused predominantly by a protonophore activity, the anionic nature of CA would likely make it a better protonophore and thus cause a stronger effect than CAME. Our experiments show the opposite effect, *i.e.*, CAME causes a much larger increase in conductance than CA (Fig. 3). Similarly, DHBA also contains a carboxylic acid group yet shows significantly less increase in conductance than CAME. The compounds CGA, SGA, and *p*CA show no increase in conductance compared to treatment with just buffer.

Second, the reduced conductance for CAME and DHBA with dietherPC further supports the presence of membrane disruption. Several landmark studies have shown that protons can migrate along the membrane surface.[69–71] This lateral transfer of protons relies upon the presence of interfacial water and is facilitated by the more stable hydrogen bonds and reduced mobility of water molecules on the membrane surface compared to bulk water.[67,72–78] Water reorientation is increased in bilayers composed of dietherPC compared to POPC[79] likely due to the lack of hydrogen bonding with the carbonyl oxygen. We would thus expect proton transfer to be increased in the presence of dietherPC. In the case of protonophore activity, this should also cause an increase in conductance. However, our data shows that replacing POPC with dietherPC reduces conductance for CAME and DHBA and does not significantly differ for CA.

In addition to protonophore activity, there are other processes we need to consider in the interpretation of our results. Weak acids can cross the membrane in their protonated forms.[80–83] The process is the same as described in the protonophore case where the compound is protonated at the water–lipid interface and permeates across the membrane in its uncharged form. Thus, at the water–lipid interface protonated and unprotonated states co-exist. Our analysis neither contradicts nor exclude this process and lipid disruption is still possible for the protonated compound. The analysis of CA and DHBA shows that the lipid–phenolic interactions are predominantly between the catechol group and the phosphate oxygen in the lipid. The carboxylic acid moiety interacts mostly with interfacial water, which is possible in the protonated or deprotonated form.

It is likely that compounds such as *p*CA, SGA and CGA that cannot cause disruption will move through the membrane in a protonated form. Again, our analysis does not exclude or contradict this. Our simulations suggest that these compounds mostly interact with interfacial water. Even in its protonated form, the carboxylic moiety is polar and capable of forming hydrogen bonds. Thus, as for the membrane-disrupting compounds, the interactions predicted by our simulations are still compatible with the model of these acids to move through the membrane in a protonated form. In fact, this is consistent with our EIS data that suggest these compounds do not induce pores, which would be the case for a compound that moves through the hydrophobic core without significantly disrupting lipid packing.

The tBLM/EIS experiments with dietherPC and DOTAP can also provide information on the role of specific phenolic–lipid interactions in altering ion membrane permeability. For all three compounds, the membrane ion permeability is significantly reduced with DOTAP compared to POPC. This suggests that the interaction with the phosphate oxygen is involved in the membrane-altering effects of CAME, CA and DHBA. The results from the MD simulations support this as they showed that all three compounds form stable interactions with the phosphate oxygen. The binding mode where the catechol group is bound to the phosphate oxygen accounts for most phenolic–lipid interactions in the simulation of CAME, CA and DHBA with POPC bilayers. Results from the tBLM/EIS experiments with dietherPC show varying effects depending on the compound. In the case of CAME, conductance is reduced by 20% with dietherPC compared to POPC. For DHBA, the reduction is 80%. In contrast, there is no significant difference in conductance between dietherPC and POPC for CA. This suggests that the carbonyl oxygen is involved in the lipid interactions of CAME and DHBA but not of CA. However, based on the simulations, none of the three compounds shows stable interactions with the carbonyl oxygen. In the case of CA, the simulation data could be a direct explanation of the lack of change in conductance between dietherPC and POPC. For CAME and DHBA, it is possible that the lack of carbonyl oxygen causes a change in how DBHA or CAME interact with the lipids, and this alternate binding mode is less effective at causing membrane disruption. As there are currently no parameters for dietherPC in the Amber force field, we cannot use simulations with this lipid to directly test these possibilities.

Table 3 provides an overview of the combined results from the tBLM/EIS experiments and the MD simulations. Despite the similarities in the structure and physico-chemical properties of the six compounds, particular the strong structural similarity of CAME, CA and *p*CA, the compounds show diverse interactions with the phospholipid bilayer. Neither the presence of the catechol group or the carboxylic group correlates with the ability to increase membrane ion permeability. The same can be said for log*P*. Based on our study of these six phenolic compounds, lipophilicity on its own cannot be used to predict whether a compound alters membrane permeability. log*P* has been found to relate to other membrane-altering activities of phenolic compounds, such as changes in the transition temperature or membrane-destabilising effects.[84] However, these effects relate to the ability of the phenolic compound to insert into the hydrophobic core, a property that is captured by log*P*. Conversely, altering the packing of lipids relates to the interaction of the compounds with lipids at the water-phospholipid interface, which is poorly captured by log*P*.

Note that simulations were carried out without an electric field. We know from test simulations carried out for previous work[17] and published work that such a weak electric field is not sufficient to induce pores in simulations. To induce pores in membranes in the absence of an electrochemical gradient, an electric field strength of 0.3 V or higher is required.[85–88] These fields are at least 10 times higher than the ones used in our experiments.

The three compounds that cause an increase in membrane permeability have the following in common: they spend most of

Table 3 Summary of results from tBLM/EIS experiments and the simulations. Details of each different property or effect can be found in the corresponding results section

Phenolic compound	Calculated log *P*	Membrane permeability	Membrane proximity	Insertion depth	Preferred orientation	Clustering	Binding mode
CAME	2.35 ± 0.02	Increase	~100%	Top of hydrophobic core	Parallel to membrane surface	Yes, clusters of two on the membrane surface	Strong preference for phosphate oxygen
CA	0.98 ± 0.02	Increase	>90%	Water–lipid interface, lipid headgroups	~45° to membrane surface	Very low tendency	Strong preference for phosphate oxygen, 'bridging' of lipids
DHBA	1.10 ± 0.13	Increase	>90%	Water–lipid interface, lipid headgroups	~45° to membrane surface	No	Strong preference for phosphate oxygen, 'bridging' of lipids
CGA	0.30 ± 0.10	No effect	74%	Interfacial water	Parallel to membrane surface	Yes, clusters of four but only one on the membrane surface	Very few interactions with lipids
SGA	1.05 ± 0.25	No effect	12%	Interfacial water	No preferred orientation	No	Very few interactions with lipids
*p*CA	0.50 ± 0.13	No effect	30%	Interfacial water	~45° to membrane surface	No	Few interactions with lipids

the time in the proximity of the membrane, where they form strong interactions with the lipid head groups rather than interfacial water. Given the small sample size, these properties are unlikely enough to predict which types of compounds can cause membrane disruption or an increase in ion membrane permeability. Nevertheless, the molecular level detail gained from our analysis allows us to provide new insight into potential mechanisms of how specific interactions at the water–lipid interface relate to membrane permeability. In our recent work, we used tBLM/EIS experiments and MD simulations to demonstrate how the differences in membrane permeability of Na^+ and K^+ ions originate from distinction coordination by carbonyl oxygens at the phospholipid–water interface.[17] Specifically, we proposed that the ability of Na^+ to create a greater number of coordinating interactions with lipids compared to K^+ causes a higher localised energy barrier for ion-induced pores, which then results in a higher membrane permeability observed in EIS experiments. We can use a similar argument to understand why CAME and CA cause an increase in membrane ion permeability while structurally similar *p*CA does not. The catechol group in CAME and CA form stable interactions with the phosphate oxygen while the methyl ester or carboxylic acid group interacts with either a second lipid or interfacial water. In both cases, the compound pushes lipids apart, causing local disruption of lipid packing and weakening the interactions between the lipids. This reduces the energy barrier for water-filed pores to be formed, thus increasing the permeability of membranes to ions. This not only increases the ion permeation, as is evident from the significant increase in conduction in our EIS experiments, but also allows the phenolic compound itself to move through the membrane in its unprotonated (charged) form. On the other hand, *p*CA does not form stable interactions with the lipid headgroup and is mostly bound to the membrane surface *via* interfacial water. This does not alter lipid packing, and hence *p*CA does not change the probability of pore formation, leaving ion membrane permeability unaltered.

The differences in binding mode between CAME compared to CA and DHBA might also explain why CAME appears to be able to wash out from the membrane easier than CA and DHBA, despite its higher log *P* value (and thus higher lipophilicity). CAME only forms interactions with a single lipid while CA and DHBA can bridge two lipids. It is possible that this makes it is easier for CAME to be washed out and for the membrane to restore its lipid packing, thus restoring membrane permeability close to baseline levels. In the case of CA and DHBA, the bridging of two lipids might make the washout and restoration of lipid packing less favorable.

5. Conclusion

We have reported the combined use of tBLM/EIS and MD simulations to study the interactions of phenolic compounds with phospholipid bilayer. Results from tBLM/EIS experiments showed that CAME, CA and DHBA significantly increase phospholipid bilayer permeability while CGA, SGA and *p*CA have no effect. Despite the similarities in the structure and physicochemical properties of the six phenolic compounds, they show diverse insertion depths, orientation, and lipid interactions. The ability to alter membrane permeability does not appear to correlate with the lipophilicity of a compound as indicated by its log *P* value. The combined results from tBLM/EIS experiments and MD simulations show that specific phenolic–lipid interactions are critical in the membrane-altering activity of CAME, CA and DHBA. Interestingly, none of the compounds that increase permeability cause a change in the structure of morphology of the phospholipid bilayer as assessed by APL or order parameters. This is consistent with our previous study of ion–lipid interactions and their role in membrane permeability. We propose that phenolic compounds can alter membrane permeability by causing local changes in lipid packing that subsequently reduce the energy barrier for ion-induced pores.

Conflicts of interest

There are no conflicts to declare.

Acknowledgements

E. D. was funded by the UTS Chancellor's Postdoctoral Fellowship scheme. This work was supported by resources provided by the Pawsey Supercomputing Centre with funding from the Australian Government and the Government of Western Australia and computational resources provided by the UTS eResearch High Performance Computer Cluster. This research was undertaken with the assistance of resources from the National Computational Infrastructure (NCI Australia), an NCRIS enabled capability supported by the Australian Government.

References

1 S. Nagar and K. Korzekwa, Drug distribution. Part 1. Models to predict membrane partitioning, *Pharm. Res.*, 2017, **34**(3), 535–543.
2 X. Liu, B. Testa and A. Fahr, Lipophilicity and its relationship with passive drug permeation, *Pharm. Res.*, 2011, **28**(5), 962–977.
3 A. Dahan and J. M. Miller, The solubility–permeability interplay and its implications in formulation design and development for poorly soluble drugs, *AAPS J.*, 2012, **14**(2), 244–251.
4 B. Funnekotter, R. L. Mancera and E. Bunn, Advances in understanding the fundamental aspects required for successful cryopreservation of Australian flora, *In Vitro Cell. Dev. Biol.: Plant*, 2017, **53**(4), 289–298.
5 A. Kaczmarczyk, *et al.*, *Current issues in plant cryopreservation, in Current frontiers in cryobiology*, InTech, 2012, pp. 417–438.
6 Y. Bagheri, A. A. Ali and M. You, Current Methods for Detecting Cell Membrane Transient Interactions, *Front. Chem.*, 2020, **8**, 603259.
7 X. Chen, *et al.*, Real-Time Structural Investigation of a Lipid Bilayer during Its Interaction with Melittin Using Sum Frequency Generation Vibrational Spectroscopy, *Biophys. J.*, 2007, **93**(3), 866–875.
8 I. M. Le-Deygen, A. A. Skuredina and E. V. Kudryashova, Experimental Methods to Study the Mechanisms of Interaction of Lipid Membranes with Low-Molecular-Weight Drugs, *Russ. J. Bioorg. Chem.*, 2020, **46**(4), 480–497.
9 H. Li, T. Zhao and Z. Sun, Analytical techniques and methods for study of drug–lipid membrane interactions, *Rev. Anal. Chem.*, 2018, **37**(1), 20170012.
10 C. Martinotti, *et al.*, Molecular dynamics simulation of the interaction of small molecules with biological membranes, *ChemPhysChem*, 2020, **21**, 1486–1514.
11 C. Ohe, *et al.*, Investigations of Polymyxin B–Phospholipid Interactions by Vibrational Sum Frequency Generation Spectroscopy, *J. Phys. Chem. B*, 2004, **108**(46), 18081–18087.
12 O. S. Ollila and G. Pabst, Atomistic resolution structure and dynamics of lipid bilayers in simulations and experiments, *Biochim. Biophys. Acta, Biomembr.*, 2016, **1858**(10), 2512–2528.
13 C. Chan and X. Cheng, *Molecular dynamics simulation studies of small molecules interacting with cell membranes, in Characterization of Biological Membranes*, De Gruyter, 2019, pp. 603–630.
14 D. Jefferies and S. Khalid, *Molecular Simulations of Complex Membrane Models, in Modeling of Microscale Transport in Biological Processes*, Elsevier, 2017, pp. 1–18.
15 C. Cranfield, *et al.*, The assembly and use of tethered bilayer lipid membranes (tBLMs), *Methods Mol. Biol.*, 2015, **1232**, 45–53.
16 A. Alghalayini, *et al.*, The use of tethered bilayer lipid membranes to identify the mechanisms of antimicrobial peptide interactions with lipid bilayers, *Antibiotics*, 2019, **8**(1), 12.
17 E. Deplazes, *et al.*, Role of Ion–Phospholipid Interactions in Zwitterionic Phospholipid Bilayer Ion Permeation, *J. Phys. Chem. Lett.*, 2020, **11**(15), 6353–6358.
18 A. Garcia, *et al.*, Label-Free, Real-Time Phospholipase-A Isoform Assay, *ACS Biomater. Sci. Eng.*, 2020, **6**(8), 4714–4721.
19 D. Bouzo, *et al.*, Characterizing the Mechanism of Action of an Ancient Antimicrobial, Manuka Honey, against Pseudomonas aeruginosa Using Modern Transcriptomics, *MSystems*, 2020, **5**(3), e00106.
20 J. M. Alvarez-Suarez, *et al.*, The Composition and Biological Activity of Honey: A Focus on Manuka Honey, *Foods*, 2014, **3**(3), 420–432.
21 F. C. Biluca, *et al.*, Phenolic compounds, antioxidant capacity and bioaccessibility of minerals of stingless bee honey (Meliponinae), *J. Food Compos. Anal.*, 2017, **63**, 89–97.
22 S. Oelschlaegel, *et al.*, Classification and characterization of manuka honeys based on phenolic compounds and methylglyoxal, *J. Agric. Food Chem.*, 2012, **60**(29), 7229–7237.
23 T. M. S. Silva, *et al.*, Phenolic compounds, melissopalynological, physicochemical analysis and antioxidant activity of jandaíra (Melipona subnitida) honey, *J. Food Compos. Anal.*, 2013, **29**(1), 10–18.
24 G. Kanimozhi and N. Prasad, Anticancer effect of caffeic acid on human cervical cancer cells, in *Coffee in health and disease prevention*, Academic Press, 2015, pp. 655–661.
25 L. Toma, *et al.*, Caffeic acid attenuates the inflammatory stress induced by glycated LDL in human endothelial cells by mechanisms involving inhibition of AGE-receptor, oxidative, and endoplasmic reticulum stress, *BioFactors*, 2017, **43**(5), 685–697.
26 Z. Lou, *et al.*, Assessment of antibacterial activity of fractions from burdock leaf against food-related bacteria, *Food Control*, 2010, **21**(9), 1272–1278.
27 Y. Sato, *et al.*, In vitro and in vivo antioxidant properties of chlorogenic acid and caffeic acid, *Int. J. Pharm.*, 2011, **403**(1–2), 136–138.
28 J. R. Colina, *et al.*, An in vitro study of the protective effect of caffeic acid on human erythrocytes, *Arch. Biochem. Biophys.*, 2019, **662**, 75–82.
29 R. C. Hider, Z. D. Liu and H. H. J. M. i. e. Khodr, Metal chelation of polyphenols, *Methods Enzymol.*, 2001, **335**, 190–203.
30 J.-P. Cornard, A. Caudron and J.-C. J. P. Merlin, UV-visible and synchronous fluorescence spectroscopic investigations

of the complexation of Al (III) with caffeic acid, in aqueous low acidic medium, *Polyhedron*, 2006, **25**(11), 2215–2222.
31 S. C. Živanović, *et al.*, The study of the influence of Mg (II) and Ca (II) ions on caffeic acid autoxidation in weakly alkaline aqueous solution using MCR-ALS analysis of spectrophotometric data, *New J. Chem.*, 2018, **42**(8), 6256–6263.
32 N. Razzaghi-Asl, *et al.*, Antioxidant properties of hydroxycinnamic acids: a review of structure-activity relationships, *Curr. Med. Chem.*, 2013, **20**(36), 4436–4450.
33 H. A. Filipe, *et al.*, Differential targeting of membrane lipid domains by caffeic acid and its ester derivatives, *Free Radical Biol. Med.*, 2018, **115**, 232–245.
34 N. P. Ulrih, A. Ota and V. J. I. J. o. F. S. Abram, Impact of selected polyphenolics on the structural properties of model lipid membranes—a review, *Int. J. Food Stud.*, 2017, **6**(2), 159–177.
35 N. P. Ulrih, *Effects of caffeic, ferulic, and p-coumaric acids on lipid membranes, in Coffee in Health and Disease Prevention*, Elsevier, 2015, pp. 813–821.
36 L. Prokai, N. M. Rivera-Portalatin and K. J. I. j. o. m. s. Prokai-tatrai, Quantitative structure-activity relationships predicting the antioxidant potency of 17β-estradiol-related polycyclic phenols to inhibit lipid peroxidation, *Int. J. Mol. Sci.*, 2013, **14**(1), 1443–1454.
37 M. H. Gordon, Dietary antioxidants in disease prevention, *Nat. Prod. Rep.*, 1996, **13**(4), 265–273.
38 J. Cejas, *et al.*, Interaction of chlorogenic acid with model lipid membranes and its influence on antiradical activity, *Biochim. Biophys. Acta, Biomembr.*, 2021, **1863**(1), 183484.
39 S. Selvaraj, *et al.*, Influence of membrane lipid composition on flavonoid–membrane interactions: implications on their biological activity, *Prog. Lipid Res.*, 2015, **58**, 1–13.
40 D. A. Case, *et al.*, *AMBER 2020*, University of California, San Francisco, 2020.
41 J. Wang, *et al.*, Development and testing of a general amber force field, *J. Comput. Chem.*, 2004, **25**(9), 1157–1174.
42 J. Wang, P. Cieplak and P. A. Kollman, How well does a restrained electrostatic potential (RESP) model perform in calculating conformational energies of organic and biological molecules?, *J. Comput. Chem.*, 2000, **21**(12), 1049–1074.
43 M. J. Frisch, *et al.*, *Gaussian 09, Revision A.02*, Gaussian, Inc., Wallingford CT, 2016.
44 A. W. S. Da Silva and W. F. Vranken, ACPYPE-Antechamber python parser interface, *BMC Res. Notes*, 2012, **5**(1), 1–8.
45 S. Kumar, *et al.*, The weighted histogram analysis method for free-energy calculations on biomolecules. I. The method, *J. Comput. Chem.*, 1992, **13**(8), 1011–1021.
46 J. S. Hub, B. L. De Groot and D. Van Der Spoel, g_wham. A Free Weighted Histogram Analysis Implementation Including Robust Error and Autocorrelation Estimates, *J. Chem. Theory Comput.*, 2010, **6**(12), 3713–3720.
47 B. Efron, Bootstrap methods: another look at the jackknife, in *Breakthroughs in statistics*, Springer, 1992, pp. 569–593.
48 E. Lindahl, *et al.*, GROMACS 2020.3, Source code, 2020.
49 Lindahl, Abraham, Hess, & van der Spoel, (2020, October 6), GROMACS 2020.4 Manual (Version 2020.4), Zenodo, DOI: 10.5281/zenodo.4054996.
50 P. Mark and L. J. T. J. o. P. C. A. Nilsson, Structure and dynamics of the TIP3P, SPC, and SPC/E water models at 298 K, *J. Phys. Chem. A*, 2001, **105**(43), 9954–9960.
51 D. A. Case, *et al.*, The Amber biomolecular simulation programs, *J. Comput. Chem.*, 2005, **26**(16), 1668–1688.
52 U. Essmann, *et al.*, A smooth particle mesh Ewald method, *J. Chem. Phys.*, 1995, **103**(19), 8577–8593.
53 L. J. P. r. Verlet, Computer ''experiments'' on classical fluids. I. Thermodynamical properties of Lennard-Jones molecules, *Phys. Rev.*, 1967, **159**(1), 98.
54 D. J. Evans and B. L. J. T. J. o. c. p. Holian, The nose–hoover thermostat, *J. Chem. Phys.*, 1985, **83**(8), 4069–4074.
55 M. Parrinello and A. Rahman, Polymorphic transitions in single crystals: A new molecular dynamics method, *J. Appl. Phys.*, 1981, **52**(12), 7182–7190.
56 W. Humphrey, A. Dalke and K. Schulten, VMD: Visual molecular dynamics, *J. Mol. Graphics*, 1996, **14**(1), 33–38.
57 N. Michaud-Agrawal, *et al.*, MDAnalysis: a toolkit for the analysis of molecular dynamics simulations, *J. Comput. Chem.*, 2011, **32**(10), 2319–2327.
58 K. Atkovska, *et al.*, Rationalizing steroid interactions with lipid membranes: Conformations, partitioning, and kinetics, *ACS Cent. Sci.*, 2018, **4**(9), 1155–1165.
59 T. Rawling, *et al.*, Aryl urea substituted fatty acids: a new class of protonophoric mitochondrial uncoupler that utilises a synthetic anion transporter, *Chem. Sci.*, 2020, **11**(47), 12677–12685.
60 N. Amdursky, *et al.*, Exploring fast proton transfer events associated with lateral proton diffusion on the surface of membranes, *Proc. Natl. Acad. Sci. U. S. A.*, 2019, **116**(7), 2443–2451.
61 Y. N. Antonenko and P. Pohl, Microinjection in combination with microfluorimetry to study proton diffusion along phospholipid membranes, *Eur. Biophys. J.*, 2008, **37**(6), 865–870.
62 M. Brändén, *et al.*, Localized proton microcircuits at the biological membrane–water interface, *Proc. Natl. Acad. Sci. U. S. A.*, 2006, **103**(52), 19766–19770.
63 E. Deplazes, *et al.*, Competing for the same space: protons and alkali ions at the interface of phospholipid bilayers, *Biophys. Rev.*, 2019, **11**(3), 483–490.
64 B. Gabriel, M. Prats and J. Teissié, Proton lateral conduction along a lipid monolayer spread on a physiological subphase, *Biochim. Biophys. Acta*, 1994, **1186**(3), 172–176.
65 T. Sandén, *et al.*, Surface-coupled proton exchange of a membrane-bound proton acceptor, *Proc. Natl. Acad. Sci. U. S. A.*, 2010, **107**(9), 4129–4134.
66 S. Serowy, *et al.*, Structural proton diffusion along lipid bilayers, *Biophys. J.*, 2003, **84**(2 Pt 1), 1031–1037.
67 M. G. Wolf, H. Grubmüller and G. Groenhof, Anomalous surface diffusion of protons on lipid membranes, *Biophys. J.*, 2014, **107**(1), 76–87.
68 T. Yamashita and G. A. Voth, Properties of hydrated excess protons near phospholipid bilayers, *J. Phys. Chem. B*, 2010, **114**(1), 592–603.
69 U. Alexiev, *et al.*, Rapid long-range proton diffusion along the surface of the purple membrane and delayed proton

transfer into the bulk, *Proc. Natl. Acad. Sci. U. S. A.*, 1995, **92**(2), 372.
70 J. Heberle, *et al.*, Proton migration along the membrane surface and retarded surface to bulk transfer, *Nature*, 1994, **370**(6488), 379–382.
71 A. Springer, *et al.*, Protons migrate along interfacial water without significant contributions from jumps between ionizable groups on the membrane surface, *Proc. Natl. Acad. Sci. U. S. A.*, 2011, **108**(35), 14461–14466.
72 M. L. Berkowitz and R. Vácha, Aqueous Solutions at the Interface with Phospholipid Bilayers, *Acc. Chem. Res.*, 2012, **45**(1), 74–82.
73 S. Y. Bhide and M. L. Berkowitz, Structure and dynamics of water at the interface with phospholipid bilayers, *J. Chem. Phys.*, 2005, **123**(22), 224702.
74 S. Y. Bhide and M. L. Berkowitz, The behavior of reorientational correlation functions of water at the water–lipid bilayer interface, *J. Chem. Phys.*, 2006, **125**(9), 094713.
75 H. Binder, Water near lipid membranes as seen by infrared spectroscopy, *Eur. Biophys. J.*, 2007, **36**(4–5), 265–279.
76 E. Deplazes, F. Sarrami and D. J. T. J. O. P. C. B. Poger, Effect of H3O+ on the Structure and Dynamics of Water at the Interface with Phospholipid Bilayers, *J. Phys. Chem. B*, 2020, **124**(8), 1361–1373.
77 E. A. Disalvo, *et al.*, Structural and functional properties of hydration and confined water in membrane interfaces, *Biochim. Biophys. Acta, Biomembr.*, 2008, **1778**(12), 2655–2670.
78 C. Zhang, *et al.*, Water at hydrophobic interfaces delays proton surface-to-bulk transfer and provides a pathway for lateral proton diffusion, *Proc. Natl. Acad. Sci. U. S. A.*, 2012, **109**(25), 9744.
79 S. Mukherjee and A. Chattopadhyay, Influence of Ester and Ether Linkage in Phospholipids on the Environment and Dynamics of the Membrane Interface: A Wavelength-Selective Fluorescence Approach, *Langmuir*, 2005, **21**(1), 287–293.
80 M. Gabba, *et al.*, Weak Acid Permeation in Synthetic Lipid Vesicles and Across the Yeast Plasma Membrane, *Biophys. J.*, 2020, **118**(2), 422–434.
81 C. Hannesschlaeger, *et al.*, The Effect of Buffers on Weak Acid Uptake by Vesicles, *Biomolecules*, 2019, **9**(2), 63.
82 S. M. Saparov, Y. N. Antonenko and P. Pohl, A new model of weak acid permeation through membranes revisited: does Overton still rule?, *Biophys. J.*, 2006, **90**(11), L86–L88.
83 A. Walter and J. Gutknecht, Monocarboxylic acid permeation through lipid bilayer membranes, *J. Membr. Biol.*, 1984, **77**(3), 255–264.
84 A. Ota, *et al.*, Interactions of p-coumaric, caffeic and ferulic acids and their styrenes with model lipid membranes, *Food Chem.*, 2011, **125**(4), 1256–1261.
85 R. A. Böckmann, *et al.*, Kinetics, statistics, and energetics of lipid membrane electroporation studied by molecular dynamics simulations, *Biophys. J.*, 2008, **95**(4), 1837–1850.
86 L. Delemotte, *et al.*, Modeling Membranes under a Transmembrane Potential, *J. Phys. Chem. B*, 2008, **112**(18), 5547–5550.
87 M. Tarek, Membrane electroporation: a molecular dynamics simulation, *Biophys. J.*, 2005, **88**(6), 4045–4053.
88 D. P. Tieleman, *et al.*, Simulation of Pore Formation in Lipid Bilayers by Mechanical Stress and Electric Fields, *J. Am. Chem. Soc.*, 2003, **125**(21), 6382–6383.

